Preprints, 4th IFAC Conference on
Advances in Proportional-Integral-Derivative Control
Almería, Spain | June 12-14, 2024

Sliding Mode Control Approach for H_2 Purity Regulation in High-Pressure Alkaline Electrolyzers

Jorge Uribe * **Edison Santillan** * **Oscar Camacho** *
Carlos Ocampo-Martinez ** **Omar Aguirre** *,**

* *Colegio de Ciencias e Ingenierías "El Politécnico", Universidad San Francisco de Quito USFQ, Quito 170157, Ecuador (e-mail: alexuribe200996@gmail.com, edison.andres68@gmail.com, {ocamacho, oaguirre}@usfq.edu.ec)*
** *Automatic Control Department, Universitat Politècnica de Catalunya - BarcelonaTECH, Barcelona, Spain (e-mail: {omar.aguirre,carlos.ocampo}@upc.edu)*

Abstract: This paper presents the design of a Sliding Mode Control (SMC) for H_2 purity regulation in high pressure alkaline electrolyzers. The control scheme is based on mixing the concepts of sliding-mode control with a PID sliding surface and Bristol matrix design. A 25-state dynamic model of the high-pressure alkaline electrolyzer is considered from the literature. The results show that the proposed control scheme design is simple, and the results obtained motivate more studies to be used in more realistic applications.

Keywords: Sliding Mode Control, Multivariable control, Decoupling, Regulation control, Nonlinear systems, Alkaline electrolysis.

1. INTRODUCTION

In the search for sustainable energy solutions, hydrogen emerges as a key player, offering promising advantages as a clean and versatile fuel. Electrolysis, a key technology in hydrogen production, has gained considerable attention as an environmentally friendly process that uses renewable energy sources (Sharma et al., 2023). However, the efficiency and reliability of electrolysis-based systems present challenges that require sophisticated control strategies. Therefore, the integration of renewable energy sources, the challenges of intermittency and the accurate control of electrolysis processes require a comprehensive exploration of control strategies (David, 2021).

The choice of a control strategy depends on the specific requirements of the electrolysis-based system, considering factors such as the dynamics of the system, the desired performance, and the level of available information regarding its framework and context of use (Qi et al., 2021; David et al., 2021). Integration of advanced control strategies can contribute significantly to the efficiency and reliability of electrolyzer technologies, especially in the context of the integration of renewable energy.

According to recent literature, the main control strategies employed for the considered systems are PID control (Qi et al., 2023), Predictive control (Huang et al., 2023), Adaptive control (Fang and Liang, 2019), Optimal control (Flamm et al., 2021), Robust control (David, 2021), Sliding Mode Control (SMC) (Yodwong et al., 2021), Fuzzy control (Shaker et al., 2022), Neural Network control (Bilgiç et al., 2023), among others. From previous control techniques, SMC has gained recognition for its robustness and ability to manage complex and non-linear systems effectively. As electrolyzers operate in dynamic and uncertain environments, adopting advanced control strategies is imperative to optimize efficiency and ensure seamless integration into evolving energy landscapes.

This article describes the development of an SMC strategy based on a sliding PID surface to regulate the purity of H_2 in high-pressure alkaline electrolyzers. The control strategy integrates the principles of both the SMC and the Bristol matrix design (Bristol, 1966). The control approach is a multivariable controller (MIMO) applied to a dynamic nonlinear model of 25 states (David et al., 2021). Therefore, the main contribution of the article is the application of the MIMO-SMC design considering the concepts of the Bristol array and applying it to the non-linear 25-state model of the electrolyzer towards maximization of the H_2 outflow purity. Note that the controller designed and proposed here considers internal variables of the electrolyzer operation. Although the purity of the H_2 outflow appears as the priority of closed-loop performance, the way to achieve such an objective is addressed by ensuring the null pressure difference among internal cameras where both gases (H_2 and O_2) are separated. Furthermore, to obtain the proper flow H_2 according to a pressure reference, another performance objective consists of minimizing the error between the pressures mentioned above.

Therefore, the controller design is simple, and the results motivate it to be used in more realistic applications. Furthermore, to the best of the authors' knowledge, the design of controllers employing the proposed method to overcome

© 2024 the authors. Accepted by IFAC for publication under a Creative Commons License CC-BY-NC-ND

the problem as mentioned above appears unaddressed in the literature.

The remainder of this paper is organized as follows. Section 2 presents the key background about electrolyzers and Sliding Mode Control; in Section 3, some modeling considerations are described; in Section 4, the proposed controller is shown; and finally, in Section 5, the simulation results with some analysis are presented.

2. PRELIMINARIES

2.1 Electrolyzer basics

Fossil fuel reserves are depleting worldwide and renewable energy sources are expected to become an important part of power generation in the near future (Kong et al., 2019). One of the problems with renewable energy is its fluctuation, as in the case of wind and solar energy, and it is necessary to find a means to store energy when production exceeds consumption. Among all renewable energy sources, hydrogen energy technology has been shown to be one of the best pathways to store and employ renewable energy. This energy vector is currently at the forefront of the revolution in energy technology, being one of the best approaches to the storage and applications of green energy (Zhao et al., 2023). Hydrogen is also considered the fuel of the future in terms of both environmental factors and energy content (Conker and Baltacioglu, 2020), which has a promising future for the care of the environment because it has lower greenhouse gas emissions (David et al., 2019).

One of the main and oldest hydrogen production technologies is water electrolysis, which is defined as the method that uses an electric current to separate a water molecule into hydrogen and oxygen, that is,

$$\mathrm{H_2O} \longrightarrow \mathrm{H_2} + \frac{1}{2}\,\mathrm{O_2}.$$

There are several methods for producing hydrogen using water electrolysis. Among the main processes, we have the following: Alkaline water electrolysis (AWE), proton exchange membrane water electrolysis (PEMWE), solid oxide water electrolysis (SOWE), and anion exchange membrane water electrolysis (AEMWE). AWE is the most cost-effective and oldest method of producing hydrogen; therefore, *alkaline electrolyzers* are more widely used around the world because they use relatively cheaper materials and have low production costs (Vidas and Castro, 2021).

Generation of *green hydrogen* involves the use of renewable energy to power electrolyzers, specifically alkaline ones, which produce clean fuel for future transportation and improve the performance of the power system. These electrolyzers act as dynamic loads and offer short-term load regulation and long-term energy storage. This proven strategy is technically and financially viable, implemented primarily in large installations connected to renewable sources such as wind or solar farms (Kiaee et al., 2018; David et al., 2019).

One of the key components of the hydrogen production process is automatic control. Controllers are important in maximizing hydrogen flow and avoiding gas contamination between hydrogen and oxygen. Controlling pressure variations within the equipment is necessary to prevent cross-contamination of potent gases, a fact that decreases the purity of the hydrogen produced (David et al., 2021).

2.2 Preliminaries for designing a Sliding Mode Contoller

Sliding Mode Control (SMC) is a nonlinear methodology under the broader Variable Structure Control (VSC) category. The SMC design process involves two main steps:

- Designing of a stable Sliding Surface: First, a sliding surface must be proposed. The choice of the sliding surface is a crucial step that depends on the model of the system and the control objectives; it defines the system's behavior.
- Designing Feedback Control: In the second phase, feedback control ensures that the system's trajectory converges to the sliding surface in a finite time and then keeps it on the sliding surface, called the *sliding mode*.

The feedback sliding mode controller consists of two parts: the continuous part $u_{eq}(t)$ and the discontinuous or nonlinear part $u_d(t)$; hence.

$$u\,(t) = u_{eq}\,(t) + u_d\,(t)\,, \tag{1}$$

- $u_d(t)$: This component drives the system from its initial state to the sliding surface. It often involves high-frequency switching dynamics to rapidly move the system toward the sliding surface.
- $u_{eq}(t)$: Once on the sliding surface, this component guides the system on the sliding surface to the desired state or trajectory. The low-frequency component stabilizes the system around the desired operating point.

Therefore, the general design methodology of SMC is described below.

- Choice of Sliding Surface: Determine the appropriate sliding surface according to the system's dynamics and control objectives.
- Determination of the Control Law: Design the feedback control law that drives the system to the sliding surface and maintains stability.
- Establishing a Convergence or Reaching Condition: Ensure that the system reaches the sliding surface in a finite time and define the stability conditions.

The reader is referred to Slotine and Li (1991); Utkin et al. (2020) as key references for a more in-depth understanding of SMC and VSC.

3. MODELING APPROACH

Electrolyzer models serve various purposes and produce results related to thermodynamics, electrochemistry, heat transfer, or gas quality. In this work, we are using the mathematical representation as proposed by David (2021). In that work, a semiphysical phenomenological model (PBSM) comprehensively represents electrolysis dynamics. A nonlinear model of 25 states is derived based on mass and energy balances. This model accurately simulates the dynamic response of hydrogen and oxygen production in a self-pressurized electrolyzer prototype. As shown in the next section, empirical modeling is suggested for controller design purposes.

3.1 Empirical modeling

In this section, an empirical multivariable (MIMO)reduced-order model obtained from the electrolyzer system model suggested by David et al. (2021), is proposed.

Hydrogen purity can be regulated when hydrogen and oxygen tank levels are controlled and pressure differences. Therefore, the system considers as variables of interest the hydrogen output pressure (P_{H_2}), the level differential (ΔL), the input voltage of the hydrogen valve (u_{H_2}), and the input voltage of the oxygen valve (u_{O_2}), see Fig. 1.

The empirical electrolyzer model proposed works around the operating point corresponding to the middle of the range as follows: tank pressure equal to 3950 KPa, hydrogen pressure similar to 4000 KPa, current density equal to 0.20979 A/cm^2, hydrogen valve voltage equal to 2.449 V, and oxygen valve voltage equal to 3.5877 V.

To obtain the system models around the operating point, step-type changes are made to the input of the process. These reference changes are positive and negative and represent 10 % of the steady-state value of the valve voltage (u_{H_2} and u_{O_2}), respectively.

As discussed beforehand, second-order models were obtained from David (2021) for P_{H_2} for both u_{H_2} and u_{O_2} inputs.The first resultant transfer function, considering a positive variation of u_{H_2}, is defined as

$$G_{11+}(s) = -46.7\frac{0.0498s + 3.96 \times 10^{-5}}{s^2 + 0.05841s + 4.506 \times 10^{-5}}. \quad (2)$$

The transfer function of ΔL for the variation of u_{H_2} is defined as

$$G_{21+}(s) = \frac{0.188689}{2239.2212s + 1}. \quad (3)$$

To obtain the system models in the event of a negative change in u_{H_2}, the same procedure is followed for positive input changes. The models obtained are defined as follows:

$$G_{11-}(s) = -57.75\frac{0.0498s + 3.96 \times 10^{-5}}{s^2 + 0.05841s + 4.506 \times 10^{-5}}, \quad (4)$$

$$G_{21-}(s) = \frac{0.106615}{1133.7205s + 1}. \quad (5)$$

To identify the system models for positive and negative variations of u_{O_2}, the procedure is analogous to the way the models were obtained for u_{H_2}. The system models in response to variations of u_{O_2} are described as follows:

$$G_{12+}(s) = -13.575\frac{0.07014s + 5.349 \times 10^{-5}}{s^2 + 0.05841s + 4.506 \times 10^{-5}}, \quad (6)$$

$$G_{22+}(s) = \frac{-0.077487e^{-1.7687s}}{1129.52s + 1}, \quad (7)$$

$$G_{12-}(s) = -14.685\frac{0.07014s + 5.349 \times 10^{-5}}{s^2 + 0.05841s + 4.506 \times 10^{-5}}, \quad (8)$$

$$G_{22-}(s) = \frac{-0.156953e^{-3.6361s}}{2273.8425s + 1}. \quad (9)$$

Therefore, $G_{11}(s)$, $G_{21}(s)$, $G_{12}(s)$ and $G_{22}(s)$ are obtained by averaging the transfer functions for both the positive and negative variations of u_{H_2} and also of u_{O_2}. They describe the behavior of the system around the previously defined operating point; see Fig. 1. The transfer functions are then the following:

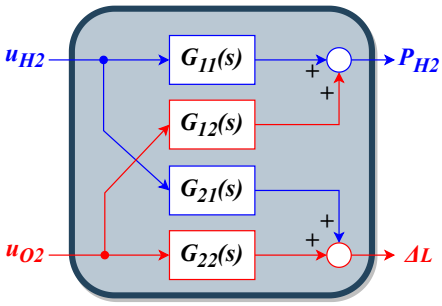

Fig. 1. Reduced-order MIMO electrolyzer system model scheme

$$G_{11}(s) = -45.8968\frac{1257.5758s + 1}{22192.632s^2 + 1296.2764s + 1}, \quad (10)$$

$$G_{21}(s) = \frac{0.147652}{1686.47s + 1}, \quad (11)$$

$$G_{12}(s) = -14.13\frac{0.07014s + 5.349 \times 10^{-5}}{s^2 + 0.05841s + 4.506 \times 10^{-5}}, \quad (12)$$

$$G_{22}(s) = \frac{-0.11722e^{-2.7024s}}{1701.6817s + 1}. \quad (13)$$

Finally, the corresponding transfer matrix of the system is defined as a system that can be expressed in the form of matrices and is defined by (14).

$$G(s) = \begin{bmatrix} G_{11}(s) & G_{12}(s) \\ G_{21}(s) & G_{22}(s) \end{bmatrix}. \quad (14)$$

3.2 Control variables pairing

The Bristol method is used to determine the pairing and interaction between the variables, and the relative gain array (RGA) of the system is obtained Bristol (1966). Then, the RGA is as follows:

$$\Lambda = G(0) \circ \left(G(0)^{-1}\right)^T, \quad (15)$$

where $G(0) = \lim_{s\to 0} G(s)$ and $\circ$ is the Hadamard product. Hence, the RGA of the system is as follows:

$$\Lambda = \begin{bmatrix} 0.684772 & 0.315228 \\ 0.315228 & 0.684772 \end{bmatrix}, \quad (16)$$

where the relationship between the input and output variables is defined as

$$\begin{bmatrix} P_{H_2} \\ \Delta L \end{bmatrix} = G(s) \begin{bmatrix} u_{H_2} \\ u_{O_2} \end{bmatrix}. \quad (17)$$

Therefore, it is determined that u_{H_2} must be paired with P_{H_2} and u_{O_2} with ΔL, similar to the one in Fig. 1.

Due to significant interaction values between variables, decouplers are designed to nullify or minimize cross-interactions between control inputs and outputs. Fig. 2 illustrates the system decoupler scheme, with the aim of removing the interaction between input $u'H_2$ and output ΔL, as well as the interaction between $u'O_2$ and P_{H_2}.

For the decoupler shown in Fig. 2, the following condition must be met to fulfill the objective of nullifying the interaction between the variables:

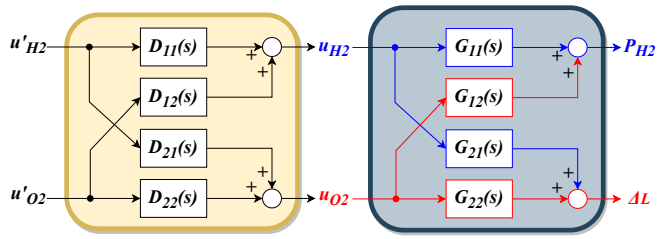

Fig. 2. System decoupling scheme

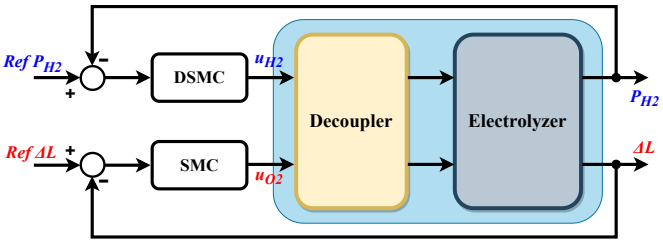

Fig. 3. Proposed Scheme based on Sliding Mode Control

$$\begin{bmatrix} G_{11} & G_{12} \\ G_{21} & G_{22} \end{bmatrix} \begin{bmatrix} D_{11} & D_{12} \\ D_{21} & D_{22} \end{bmatrix} = \begin{bmatrix} Q_{11} & 0 \\ 0 & Q_{22} \end{bmatrix}, \tag{18}$$

where Q_{11} and Q_{22} are the decoupled system outputs. Solving (18), it yields

$$D = \begin{bmatrix} 1 & -\dfrac{G_{12}}{G_{11}} \\ -\dfrac{G_{21}}{G_{22}} & 1 \end{bmatrix}. \tag{19}$$

Considering that the decoupler is going to be static, and taking into account the steady-state gains of the system then the system decoupler is described as follows:

$$D = \begin{bmatrix} 1 & -0.36546 \\ 1.2596 & 1 \end{bmatrix}. \tag{20}$$

4. PROPOSED CONTROLLER APPROACH

The design of the controllers for P_{H_2} and ΔL will be based on the reduced-order models in (10) and (13), respectively. The proposed SMC architecture for the electrolyzer system is shown in Fig. 3.

4.1 Controller design for the level loop

The transfer function of the level for u_{O_2} is represented by the FOPDT model in (13), for which the SMC controller design is as follows.

From (13),

$$G_{22}(s) = \frac{Ke^{-t_0 s}}{\tau s + 1} = \frac{Y(s)}{U(s)} \cong \frac{K}{(\tau s + 1)(t_0 s + 1)}. \tag{21}$$

Computing the corresponding time-domain expression of (21), it yields

$$\frac{d^2 y(t)}{dt^2} + a_1 \frac{dy(t)}{dt} + a_2 y(t) = K_g u(t), \tag{22}$$

where

$$K_g = \frac{K}{\tau t_0}, \quad a_1 = \frac{\tau + t_0}{\tau t_0}, \quad \text{and} \quad a_2 = \frac{1}{\tau t_0}. \tag{23}$$

From (22), the sliding surface of the controller is defined as follows:

$$\begin{aligned} \sigma(t) &= \left(\frac{d}{dt} + \lambda\right)^2 \int_0^t e(t)dt \\ &= \frac{de(t)}{dt} + 2\lambda e(t) + \lambda^2 \int_0^t e(t)dt, \end{aligned} \tag{24}$$

where the error, namely $e(t)$, is defined by the arithmetic subtraction between the reference $r(t)$ and the system response $y(t)$, i.e., $e(t) \triangleq r(t) - y(t)$.

Since the goal of the sliding surface is to make the error null, the following condition must be met:

$$\frac{d\sigma(t)}{dt} = 0 = \frac{d^2 e(t)}{dt^2} + 2\lambda \frac{e(t)}{dt} + \lambda^2 e(t). \tag{25}$$

Performing the proper rewriting of expressions based on previous definitions and solving for the highest-order derivative of the controlled variable, it yields

$$\frac{d^2 y(t)}{d^2 t} = \frac{d^2 r(t)}{dt} + 2\lambda\left(\frac{dr(t)}{dt} - \frac{dy(t)}{dt}\right) + \lambda^2 e(t). \tag{26}$$

Replacing (26) into (22), removing the derivatives from the reference, and solving for the control variable, the equivalent part of the SMC controller is defined as

$$u_{eq}(t) = \frac{1}{K_g}\left(\frac{dy(t)}{dt}(a_1 - 2\lambda) + \lambda^2 e(t) + a_2 y(t)\right). \tag{27}$$

By changing the variable λ to $\frac{a_1}{2}$, the equivalent action of the SMC is reduced to

$$u_{eq}(t) = \frac{1}{K_g}\left(\frac{a_1^2}{4} e(t) + a_2 y(t)\right). \tag{28}$$

On the other hand, the discontinuous component of the SMC is described by

$$u_d = k_d \frac{\sigma(t)}{|\sigma(t)| + \delta}. \tag{29}$$

The tuning values considered are taken from Camacho and Smith (2000), being

$$k_d = \frac{0.51}{|K|}\left(\frac{\tau}{t_0}\right)^{0.76} \quad \text{and} \quad \delta = 0.68 + 0.12\,|K|\,k_d a_1.$$

Finally, with the objective of smoothing and including the controller action(24), the sliding surface takes the following form (Camacho and Smith (2000)):

$$\sigma(t) = \text{sign}(K)\left(-\frac{dy(t)}{dt} + 2\lambda e(t) + \lambda^2 \int_0^t e(t)dt\right). \tag{30}$$

4.2 Controller design for the pressure loop

The transfer function adapted from the hydrogen pressure response for u_{H_2} is represented by a second-order model with zero.

From (10),

$$G_{11}(s) = K\frac{\tau_3 s + 1}{\tau_1 s^2 + \tau_2 s + 1}. \tag{31}$$

Computing the corresponding time-domain expression for (31), it yields

$$\tau_1 \frac{d^2 y(t)}{dt} + \tau_2 \frac{dy(t)}{dt} + y = K\tau_3 \frac{du(t)}{dt} + Ku(t). \tag{32}$$

Equation (32), like (22), is a second-order differential equation, then the corresponding sliding surface will have

the same structure as in (24). Hence, substituting (26) into (32) results in

$$\tau_1 \frac{d^2 r(t)}{d^2 t} + 2\lambda \frac{dr(t)}{dt} + \frac{dy(t)}{dt}(\tau_2 - 2\lambda\tau_1) + \ldots \\ \ldots + y(t) + \tau_1 \lambda^2 e(t) = K\tau_3 \frac{du(t)}{dt} + Ku(t). \tag{33}$$

By performing the change of variable $\lambda = \frac{\tau_2}{2\tau_1}$, removing the second derivative of the reference and solving for the derivative of the control variable, the equivalent part of the DSMC is defined as

$$\frac{du_{eq}}{dt} = \frac{1}{K\tau_3}\left(\frac{\tau_2}{\tau_1}\frac{dr}{dt} + y + \frac{\tau_2^2}{4\tau_1}e - Ku_{eq}\right). \tag{34}$$

The discontinuous part of the dynamic SMC controller (DSMC) corresponds with (Espin et al., 2022)

$$\frac{du_d}{dt} = k_d \text{sign}(S). \tag{35}$$

The suggested tuning parameters are determined as

$$k_d = \frac{0.51}{|K|}\left(\frac{\tau}{t_0}\right)^{0.76}\left(\frac{\tau_1}{\tau_2 + \tau_3}\right),$$

with the equivalent time constant and dead time as follows:

$$\tau = \tau_2 - 0.5\left(\tau_2 \pm \sqrt{\tau_2^2 - 4\tau_1}\right),$$

and

$$t_0 = 0.5\left(\tau_2 \pm \sqrt{\tau_2^2 - 4\tau_1}\right).$$

The tuning parameters for the designed SMC and DSMC controllers are shown in Table 1.

Table 1. Controllers Tuning Values

Parameter	SMC	DSMC
λ	0.185314	2.9205×10^{-2}
k_d	583.3192	2.5357
δ	3.72109	–

5. SIMULATION RESULTS AND DISCUSSION

This section discusses the results obtained by simulating the proposed controllers considering the dynamic model of 25 states of a high-pressure alkaline electrolyzer reported in David et al. (2021).

Rejection tests of disturbances in the current density were performed to show the benefits and effectiveness of the proposed approach for the electrolyzer system ; Fig. 4 shows the disturbances that occur at the current density. It should be noted that the scales of the images are the same as those presented by David et al. (2021).

In this simulation, the electrolyzer produces gases at constant pressure, but the electric current fluctuates as if renewable energy sources provided it. The current density changes in this case while the pressure reference is kept constant.

The objective of the control scheme is to keep the pressure reference $P_{H_2}^{\text{ref}}$ fixed at 4000 KPa, while the differential reference level ΔL^{ref} is maintained at 0 mm. It can be seen

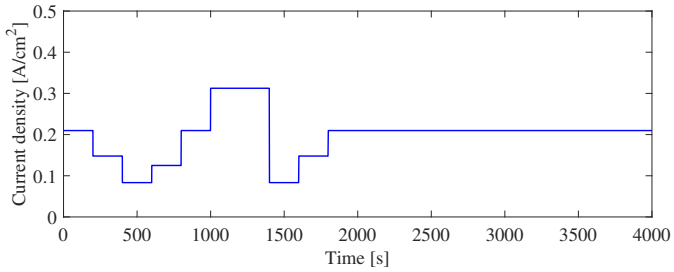

Fig. 4. Disturbances in the current density

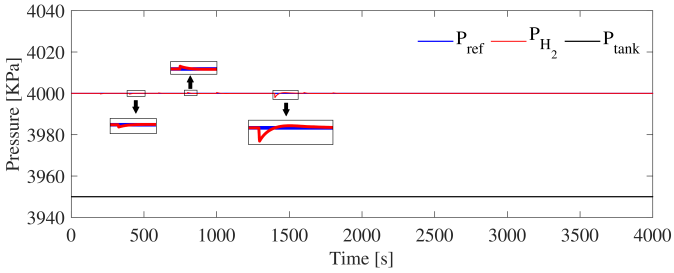

Fig. 5. System pressure response to current density disturbances

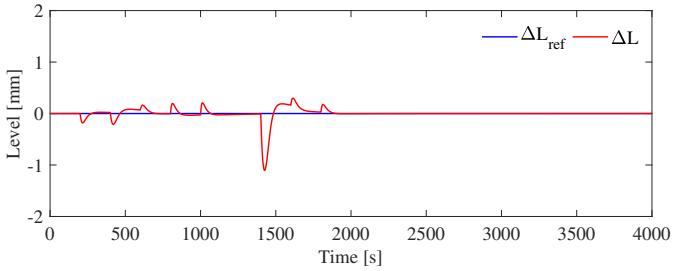

Fig. 6. System level response to current density disturbances

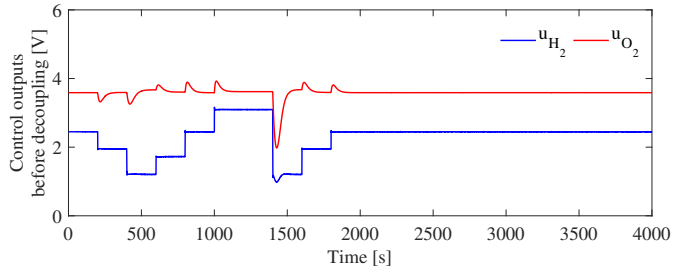

Fig. 7. Controller actions

that despite the disturbances, the variations in pressure and level are imperceptible, as seen in Figs. 5 and 6.

Figure 7 shows the control actions of the SMC (u_{O_2}) and the DSMC (u_{H_2}); overall, the output of both controllers responds quickly, being u_{O_2} with a smaller variation in amplitude than that produced by u_{H_2}, so in this case, it should improve the tuning in future works. Something important for SMC controllers is that both are without chattering in the controllers' actions. The smoothed version of the SMC works well, as the DSMC. Therefore, they do not reduce the useful life of the final control element, which is one of the main problems with SMC.

Due to the effective performance of the controllers, the impurity O_2, with its highest value, remains consistently below 1%, as shown in Fig. 8.

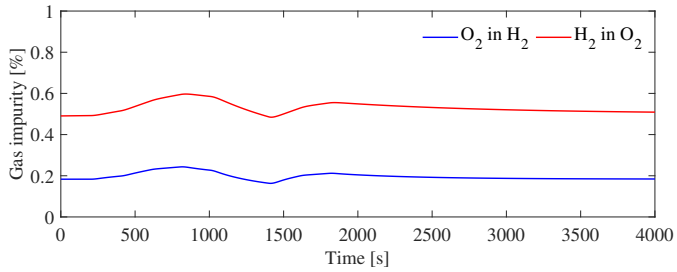

Fig. 8. Gas impurity percentage

The results match closely those reported in David et al. (2021), but with less pronounced fluctuations in pressure and level output. The u_{O_2} controller shows fewer amplitude variations, while the u_{H_2} controller aligns with the one obtained in the referenced paper.

In future studies, our aim is to explore additional scenarios and conduct more experiments with parameter variations. This article focuses on a single case due to space constraints, but these initial results motivate more extensive research and analysis in subsequent work.

ACKNOWLEDGEMENTS

Jorge Uribe and Edison Santillan are thankful for the research internship at the USFQ Advanced Control Systems Research Group, Quito, Ecuador. This work has been partially supported by the Spanish project L-BEST (PID2020-115905RB-C21) funded by the Ministry of Science and Innovation (MCIN/AEI/10.13039/501100011033).

REFERENCES

Bilgiç, G., Bendeş, E., Öztürk, B., and Atasever, S. (2023). Recent advances in artificial neural network research for modeling hydrogen production processes. *International Journal of Hydrogen Energy*.

Bristol, E. (1966). On a new measure of interaction for multivariable process control. *IEEE transactions on automatic control*, 11(1), 133–134.

Camacho, O. and Smith, C.A. (2000). Sliding mode control: an approach to regulate nonlinear chemical processes. *ISA transactions*, 39(2), 205–218.

Conker, C. and Baltacioglu, M.K. (2020). Fuzzy self-adaptive pid control technique for driving hho dry cell systems. *International Journal of Hydrogen Energy*, 45(49), 26059–26069.

David, M., Bianchi, F., Ocampo-Martinez, C., and Sánchez-Peña, R. (2021). Model-based control design for h2 purity regulation in high-pressure alkaline electrolyzers. *Journal of the Franklin Institute*, 358(8), 4373–4392.

David, M., Ocampo-Martinez, C., and Sánchez-Peña, R. (2019). Advances in alkaline water electrolyzers: A review. *Journal of Energy Storage*, 23, 392–403.

David, M.R. (2021). *Mathematical modelling and advanced control design applied to high-pressure electrolyzers for hydrogen production*. Ph.D. thesis, Universitat Politécnica de Catalunya. URL `http://hdl.handle.net/10803/675532`.

Espin, J., Castrillon, F., Leiva, H., and Camacho, O. (2022). A modified smith predictor based–sliding mode control approach for integrating processes with dead time. *Alexandria Engineering Journal*, 61(12), 10119–10137.

Fang, R. and Liang, Y. (2019). Control strategy of electrolyzer in a wind-hydrogen system considering the constraints of switching times. *International journal of hydrogen energy*, 44(46), 25104–25111.

Flamm, B., Peter, C., Büchi, F.N., and Lygeros, J. (2021). Electrolyzer modeling and real-time control for optimized production of hydrogen gas. *Applied Energy*, 281, 116031.

Huang, C., Zong, Y., You, S., Træholt, C., Zheng, Y., Wang, J., Zheng, Z., and Xiao, X. (2023). Economic and resilient operation of hydrogen-based microgrids: An improved mpc-based optimal scheduling scheme considering security constraints of hydrogen facilities. *Applied Energy*, 335, 120762.

Kiaee, M., Infield, D., and Cruden, A. (2018). Utilisation of alkaline electrolysers in existing distribution networks to increase the amount of integrated wind capacity. *Journal of Energy Storage*, 16, 8–20.

Kong, L., Yu, J., and Cai, G. (2019). Modeling, control and simulation of a photovoltaic/hydrogen/supercapacitor hybrid power generation system for grid-connected applications. *International Journal of Hydrogen Energy*, 44(46), 25129–25144.

Qi, R., Gao, X., Lin, J., Song, Y., Wang, J., Qiu, Y., and Liu, M. (2021). Pressure control strategy to extend the loading range of an alkaline electrolysis system. *International Journal of Hydrogen Energy*, 46(73), 35997–36011.

Qi, R., Li, J., Lin, J., Song, Y., Wang, J., Cui, Q., Qiu, Y., Tang, M., and Wang, J. (2023). Design of the pid temperature controller for an alkaline electrolysis system with time delays. *International Journal of Hydrogen Energy*, 48(50), 19008–19021.

Shaker, F.N., Obed, A.A., and Abid, A.J. (2022). Comprehensive design for a neuro-fuzzy controller for a safe hydrogen energy storage. In *2022 10th International Conference on Smart Grid (icSmartGrid)*, 124–130. IEEE.

Sharma, G.D., Verma, M., Taheri, B., Chopra, R., and Parihar, J.S. (2023). Socio-economic aspects of hydrogen energy: An integrative review. *Technological Forecasting and Social Change*, 192, 122574.

Slotine, J.J.E. and Li, W. (1991). *Applied nonlinear control*. Prentice hall Englewood Cliffs, NJ.

Utkin, V., Poznyak, A., Orlov, Y.V., and Polyakov, A. (2020). *Road map for sliding mode control design*. Springer.

Vidas, L. and Castro, R. (2021). Recent developments on hydrogen production technologies: state-of-the-art review with a focus on green-electrolysis. *Applied Sciences*, 11(23), 11363.

Yodwong, B., Guilbert, D., Kaewmanee, W., Phattanasak, M., Hinaje, M., and Vitale, G. (2021). Modified sliding mode-based control of a three-level interleaved dc-dc buck converter for proton exchange membrane water electrolysis. In *2021 Research, Invention, and Innovation Congress: Innovation Electricals and Electronics (RI2C)*, 221–226. IEEE.

Zhao, M.J., He, Q., Xiang, T., Ya, H.Q., Luo, H., Wan, S., Ding, J., and He, J.B. (2023). Automatic operation of decoupled water electrolysis based on bipolar electrode. *Renewable Energy*, 203, 583–591.